Proc. Natl. Acad. Sci. USA
Vol. 93, pp. 2749–2754, April 1996
Biochemistry

Batimastat, a potent matrix metalloproteinase inhibitor, exhibits an unexpected mode of binding

(metastasis/drug design/crystallography/molecular modeling)

ISTVAN BOTOS*, LEONARDO SCAPOZZA*, DACHUAN ZHANG*, LANCE A. LIOTTA†, AND EDGAR F. MEYER*‡

*Biographics Laboratory, Department of Biochemistry and Biophysics, Texas A&M University, College Station, TX 77843-2128; and †Laboratory of Pathology, National Cancer Institute, Bethesda, MD 20892

Communicated by Derek H. R. Barton, Texas A&M University, College Station, TX, November 30, 1995 (received for review April 21, 1995)

ABSTRACT **Matrix metalloproteinase enzymes have been implicated in degenerative processes like tumor cell invasion, metastasis, and arthritis. Specific metalloproteinase inhibitors have been used to block tumor cell proliferation. We have examined the interaction of batimastat (BB-94) with a metalloproteinase [atrolysin C (Ht-d), EC 3.4.24.42] active site at 2.0-Å resolution (R = 16.8%). The title structure exhibits an unexpected binding geometry, with the thiophene ring deeply inserted into the primary specificity site. This unprecedented binding geometry dramatizes the significance of the cavernous primary specificity site, pointing the way for the design of a new generation of potential antitumor drugs.**

Extracellular matrix cleavage is a critical component of many physiological and pathological conditions. These processes may be differentiated by the way in which extracellular matrix turnover is regulated. Many pathological conditions are distinguished by uncontrolled matrix degradation that results in excessive tissue destruction, disruption of matrix boundaries, and loss of extracellular matrix function. The matrix metalloproteinases (MMPs; ref. 1) have been implicated in both physiological and pathological remodeling.

MMP expression has been correlated with the invasive phenotype in a variety of human tumors (2), including human breast, colon, thyroid, hepatocellular, lung, and prostate cancers. These studies have included both immunohistochemical and *in situ* hybridization analyses. Recently, these studies have been refined to examine the role of MMP-2 (72 kDa; type IV collagenase and gelatinase A) in the process of tumor cell invasion in human breast and lung cancers (3, 4). Inhibition of MMP activity, in particular MMP-2 activity, has also demonstrated a direct role for this enzyme in tumor cell invasion and angiogenesis (4–6). While crystal structures of type IV collagenase are not available, sequence similarities have been used to create working models for docking experiments, based on the structurally determined MMPs [MMP-1, 3, 8 (7–9)], which are associated with degenerative diseases (arthritis, corneal ulceration, and periodontitis). Mammalian MMPs are also involved with normal cellular physiology and remodeling. Because of a common physiological characteristic, the ability to penetrate the extracellular matrix (10), the snake venom (*Crotalus atrox*) MMP atrolysin C (Ht-d, EC 3.4.24.42) was used to explore the nature of inhibitor binding.

As this family of enzymes continues to be studied crystallographically, common features can be identified and used for structure-based inhibitor design. The conserved isostructural (11) sequence (HEXXHXXGXXH) creates a common locus for the active site Zn atom and an exceptionally large and deep S1′ pocket (12) as part of the extended binding site for collagen-like substrates; mammalian and venom MMPs exhibit (13) a striking structural similarity (Table 1). With the exception of MMP-1, which has an Ile-144 → Arg replacement at the mouth of the S1′ pocket and thus limits its specificity to small hydrophobic residues, the MMPs can accept large extended functional groups at the S1′ locus. Crystallographic data of inhibitors bound to MMP-1, 3, and 8 show that the S1′ pocket is only minimally filled by natural and synthetic side chains; the exception to this being the title complex and two recently reported structures (8, 14), which exhibited greater occupancy of the S1′ pocket.

Under physiological conditions batimastat (BB-94)

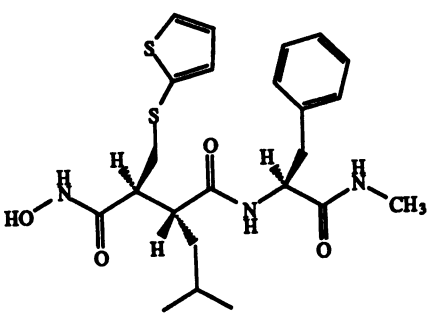

Scheme I

inhibits gelatinases A and B (6) with IC_{50} values of 4 nM and 10 nM, respectively. The IC_{50} with the structurally similar collagenase Ht-d (14) is 6 nM, which is comparable with values for MMP-1 (3 nM), MMP-8 (10 nM), and MMP-3 (20 nM). Intraperitoneal administration of BB-94 effectively blocked growth of human ovarian carcinoma xenografts (15) and murine melanoma metastasis (16) and delays the growth of primary tumors in an orthotopic model of human breast cancer (W. G. Stetler-Stevenson, personal communication) without cytotoxicity and without affecting mRNA levels (17). Cocrystallization studies (ref. 18; K. Appelt, personal communication) with the truncated fibroblast and neutrophil collagenases (MMP-1 and MMP-8) indicated that BB-94 inhibition is derived from hydroxamate binding to the catalytic Zn atom and favorable adaptation to the extended binding sites.

The results of this study reveal an unexpected binding geometry that shows alternative Zn ligation and van der Waals interactions, especially in the pronounced S1′ (12) primary specificity pocket; they thus provide novel insight for the development of new inhibitors for the treatment of collagenase-linked diseases.

MATERIALS AND METHODS

Crystallographic Studies. BB-94 (lot 91L033) was supplied by British Biotechnology, Oxford, U.K. as a dry white powder

The publication costs of this article were defrayed in part by page charge payment. This article must therefore be hereby marked "*advertisement*" in accordance with 18 U.S.C. §1734 solely to indicate this fact.

Abbreviations: BB-94, batimastat; Ht-d, atrolysin C, form d (EC 3.4.24.42); MMP, matrix metalloproteinase.

‡To whom reprint requests should be addressed.

§The atomic coordinates have been deposited in the Protein Data Bank, Chemistry Department, Brookhaven National Laboratory, Upton, NY 11973 (reference 1DTH).

Table 1. rms deviation between three MMPs

	rms deviation, Å		
	Ht-d	MMP-1	MMP-8
Ht-d	0	0.99	1.04
MMP-1	0.99	0	0.56

Two hundred seventy-two backbone atoms (extended binding site) were superimposed.

with limited aqueous solubility (<2.5 mg/ml). Purified Ht-d was provided by Jay Fox (University of Virginia Health Science Center, Charlottesville). A single crystal (0.4 × 0.4 × 1.5 mm) of Ht-d, obtained as reported (14) [0.1 M imidazole buffer, pH 6.8/2.4 M $(NH_4)_2SO_4$], was placed in a 0.5-mm-diameter capillary in the presence of buffer saturated from a solid lump of BB-94 placed at one end of the needle-like crystal ($a = b = 97.21$ Å, $c = 87.91$ Å; $P6_5$). Cu–Kα radiation was used to collect diffraction data over a crystal rotation range of 96° (1.2° per step) to 2.0-Å resolution with a Rigaku R-AXIS IIc area detector (Table 2) and was evaluated with the program DENZO (19). No evidence of radiation decay was observed (scale factors from frame 0 to 60 vary by less than 10%). The data compared with native Ht-d data measured from a fresh crystal has an R_{merge} of 12%.

The difference Fourier map (Fig. 1) phased with the refined native structure (with active-site water removed) showed clear electron density for BB-94 in the active site. Two strong (5σ) peaks deep in the S1′ pocket uniquely identified the locations of the two S atoms of BB-94. A simulated annealing calculation of the native dimer removed possible bias of side-chain orientations; the structure was refined [X-PLOR (20)] at 2.0 Å (R = 22%). Outside the active site, 152 water molecules were added; further refinement gave R = 18%.

The resulting difference Fourier map clearly revealed an elongated electron density shape in the active site, corresponding to the inhibitor in an extended conformation. A model of the inhibitor optimized with MOPAC 6.0 (21) was adjusted to fit residual density in the active site. Amino acid side-chain positions were adjusted by using program PRONTO (A. Laczkowski and S. M. Swanson, unpublished computer program), based on statistics provided by the program PROCHECK (22). The complex was further refined; water molecules adjacent to the inhibitor were identified and included in the final model (R = 16.8%). During this refinement process, the independent "free" R factor (20), increased initially (29.8%) before decreasing monotonically to 27.2%.

Modeling. The volumes of the S1′ (12) cavity and of the molecular surface envelope were calculated with the molecular modeling program GRASP (23) by using the atomic coordinates from the x-ray structure of Ht-d (14) and of human MMP-8 (9), with water molecules removed from the extended binding site. The refined atomic coordinates of BB-94 were used for the molecular surface calculation. Electrostatic potentials were calculated by using the program DELPHI (24). Starting with the BB-94 conformation optimized by using the PM3 Hamiltonian function (25) of MOPAC, potential-derived atomic charges for DELPHI input were computed by a single-point SCF calculation at the MNDO (26) level.

The program GRID (27) was used to calculate the interaction energies between several probes (N1, neutral flat NH amide group; O, sp^2 carbonyl oxygen atom; C3, neutral methyl group) and the empty extended binding sites of Ht-d and MMP-8 (18), obtained by excluding the complexed inhibitor and structurally nonsignificant water molecules. A regular three-dimensional array of grid points separated by 0.5 Å was established throughout and around the whole protein to enclose the entire binding site. Interaction energies were calculated from a simple Lennard–Jones potential energy function (27) at regularly spaced points of the three-dimensional grid, with a cutoff of 5 kcal/mol for repulsive energies. Contour maps at negative and zero kcal/mol interaction energy levels were displayed on an E&S ESV graphic workstation (PRONTO; A. Laczkowski and S. M. Swanson, unpublished computer program) to depict energetically favorable sites for known and putative inhibitors.

Table 2. Crystallographic and refinement data for BB-94

Area detector	R axis
Total reflections, no.	222,723
Unique reflections, no.	36,261
R_{merge}, %	6.3
Resolution range for refinement, Å	8.0–2.0
Data completeness, %	92.6
Highest-resolution shell, Å	2.1–2.0
Data completeness, %	88.2
No. of atoms in refinement	4,886
R factor, %	16.8
rmsd bonds, Å	0.01
rmsd angles, degrees	2.19

rmsd, rms deviation. $R_{merge} = [\Sigma_{hkl}\Sigma_{refl}|I(hkl,j) - \overline{I}(hkl)|/\Sigma_{hkl}\Sigma_{refl}|I(hkl,j)|] \times 100\%$. R factor $= (\Sigma||F_{obs}| - |F_{calc}||/\Sigma|F_{obs}|) \times 100\%$.

RESULTS

Crystallography. The difference Fourier map (Fig. 1) clearly shows that BB-94 is deeply inserted into the S1′ site,

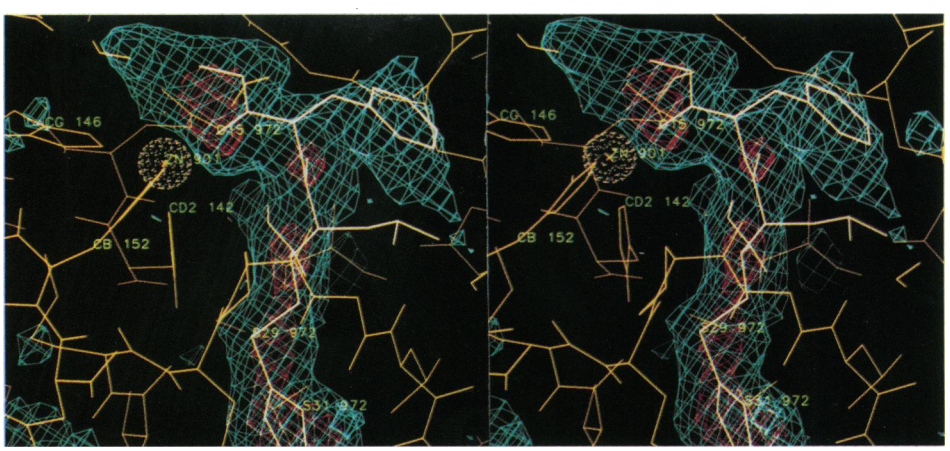

FIG. 1. Initial unbiased difference Fourier ($F_{obs} - F_{calc}$) electron density map in the active site region [at 2.0σ (blue) and 5σ (red)] is shown in stereo. BB-94 (white) has been fit to density by using PRONTO (A. Laczkowski and S. M. Swanson, unpublished computer program) in an extended conformation.

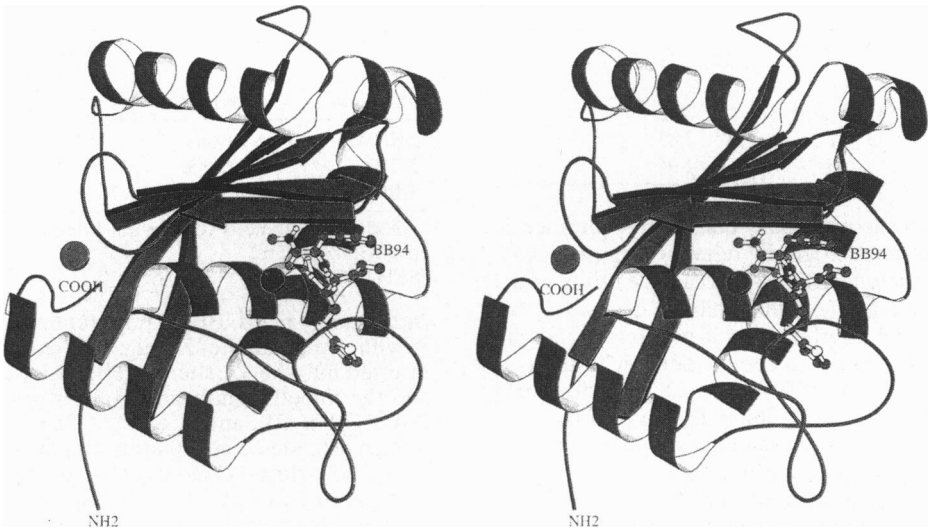

FIG. 2. Stereo ribbon diagram of Ht-d (MOLSCRIPT; ref. 28). The catalytic Zn atom (dark sphere), the structural Ca, and BB-94 are shown as a ball-and-stick model.

with the terminal methylamide group ligating the active site Zn atom (Zn · · · NE2 His, 1.95–2.09 Å; Zn · · · O15 BB-94, 1.95–2.01 Å) and the Phe side chain splayed favorably into the S′ region of the extended binding site (Fig. 2). The thiophene ring reaches near the bottom of the hydrophobic S1′ pocket (Fig. 3), which is lined by main-chain H-bonding atoms (N and O) but is devoid of charged residues. As expected, the thiophene S atom has the strongest peak in the difference Fourier map, enhanced by the extended heterocyclic π electron system. H bonds (Table 3) between the inhibitor and the enzyme give additional significance to the shape and orientation of individual functional groups. The extraordinary size and shape of the S1′ pocket (Fig. 3) of MMPs is fully utilized in this complex and is thus worthy of further consideration. Two structure determinations of S1′-bound aromatic moieties (14) first indicated that the S1′ pocket of many MMPs can be more fully occupied (29) than in the case of naturally occurring amino acids (Table 4). A peptidomimetic inhibitor bound to human MMP-3 (8) further confirmed this observation. Moreover, there is clear evidence of a direct relationship between inhibitory potential and the ability to fill the pocket (30). An opening at the "bottom" of the pocket and a localized water molecule (HOH 728) indicate the functional role of bound water in such pockets, which has been recognized (31) to be a conserved structural feature in a number of protein molecules and in this example provides the felicitous function of allowing bound water displaced by bulky ligand binding to be ejected entropically and reversibly into bulk solvent, further enhancing binding affinity.

Modeling. Two crucial characteristics dominate ligand binding (and thus provide valuable insight for subsequent inhibitor design): Zn ligation and optimal occupancy of the primary specificity (S1′) site. The title complex differs significantly from those obtained from cocrystallization under low-salt conditions employed by two other crystallographic groups, which show the hydroxamate moiety ligating to Zn and the Leu side chain occupying the S1′ pocket (ref. 18; K. Appelt, personal communication). The title complex shows a completely different binding mode, even though the active site structures of the venom and human enzymes (9, 14) are topologically identical. For this reason we compared the S1′ cavity volume and shape of Ht-d with that of MMP-8 (coordinates courtesy of W. Bode, Max-Planck-Institut für Biochemie, Martinsried, Germany). This comparison (Fig. 4) reveals that despite a virtually superimposable peptide backbone scaffold, the S1′ pocket of Ht-d has a differently shaped entrance and has a 23% larger volume than the corresponding pocket of MMP-8. This comparison suggests that while Ht-d exhibits complete occupancy of the S1′ pocket, it would be unlikely for BB-94 to bind to human MMP-8 in the same

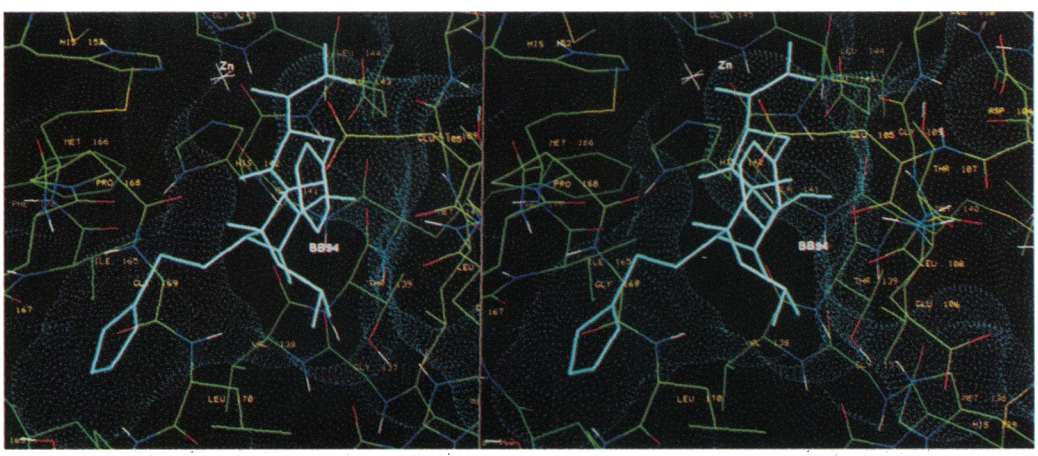

FIG. 3. Connoly surface (1.4-Å probe) of the extended binding site (INSIGHT II, Biosym Technologies, San Diego), with BB-94 (cyan). The residues defining the S1′ and S2′ sites are labeled. The average temperature factors of inhibitor atoms (30 Å^2 at 90% occupancy) are commensurate with those of the whole protein (25 Å^2).

Table 3. Inhibitor–protein hydrogen bonds

Donor	Acceptor	Distance, Å
N 16-I	O 109	2.90
O 38-I	OE2 143	3.02
O 38-I	O 139	2.83
N 18-I	O 168	2.94

orientation because of the marginally constricted entrance of the pocket. While not physiologically relevant (high salt buffer), the title structure serendipitiously reveals the utility of the overlarge S1′ pocket as a target for inhibitor design for this family of enzymes; modeling efforts now in progress permit the design of alternative P1′ moieties complementary to marginally differentiated pockets in MMP-1, 3, and 8 and, thus, form the structural basis for current inhibitor design efforts.

To understand why the hydroxamate group is not the dominant factor in binding and does not dictate the expected binding orientation in the case of the title complex, we analyzed (DELPHI) the charge distribution of BB-94 as a function of the ionic strength of the buffer. This analysis permits us theoretically to simulate the different reaction conditions used for the Ht-d and MMP-8 complexes with BB-94. The result (Fig. 5) reveals that the difference between the charge distribution of methylamide and hydroxamate groups becomes less important with increasing ionic strength of the buffer or solvent. Therefore, contrary to the low salt condition, in high salt buffer soaking conditions (Ht-d), the methylamide moiety has approximately the same affinity for Zn ligation as the hydroxamate group. In this context the experimental results indicate that van der Waals interactions, primarily in the S1′ pocket, then play the major role in determining the binding orientation of the inhibitor. Because of potential toxicity associated with the popular hydroxamate moiety, this observation is additionally relevant for future inhibitor design strategies, where other ligands will be exploited, especially those (e.g., phosphonates) permitting occupancy of both S and S′ regions.

Another question raised by the unexpected binding mode is whether the determined orientation allows the discrimination between the active form (*S,R,S*)[¶] of BB-94 (K_i = 6 nM) and BB-1268, the 670-fold less potent enantiomer of BB-94 (*R,S,R*)[‖] (15). To answer this question, both enantiomers were docked into the active sites of Ht-d and MMP-8 by using the GRID energy maps. BB-94 preferentially binds to MMP-3 and 8 with hydroxamate–Zn ligation and the Leu side chain inserted into the S1′ site; the Phe residue occupies the S2′ site and the thioethylthiophene chain is oriented as a cover over Pro-217, His-201, and His-207.** The inhibitor backbone thus is in an extended conformation and the carbonyl oxygen (O15, O20), the hydroxyl O atom (O38), and the N atom (N37) would form H bonds with the corresponding H-bond donor or acceptor atoms of the peptide backbone of the protein. The same docking experiment was repeated for both orientations (thiophene or Leu in S1′) by using the MOPAC PM3 energy minimized structure of the inactive enantiomer (BB-1268). For the latter test, the Zn chelation and the backbone conformation were maintained in the same position as in the model of the active inhibitor complex to conserve favorable interactions. The results for the orientation with Leu in S1′ show that it is not possible to completely fit the side chains of the inactive compound into the calculated energetically favorable sites of Ht-d and MMP-8 because of unfavorable steric repulsions. This is in agreement with the difference in the effectiveness of binding being a discriminator for inhibitory activity. Docking the thiophene into S1′ shows the same result described for the other orientation (Leu in S1′). Trying to fit the inactive enantiomer of BB-94 into the experimentally determined electron density from a difference Fourier (omit) map proved to be impossible. In conclusion, the results of the docking experiment with the unexpected fit show that the experimentally determined orientation can discriminate between the two enantiomers in the same manner as the reported MMP-8 complex.

Table 4. Extent of inhibitor interaction with S1′ pocket

Inhibitor	Source	Occluded volume in S1′ pocket, Å^3	Interaction surface with protein, Å^2
pENW*	Natural	201	140
SCH†	Synthetic	162	160
BB94	Synthetic	83	240

Occluded volume is volume not filled by inhibitor.
*pyroGlu-Asn-Trp.
†SCH47890.

DISCUSSION

Two unlikely events [choice of a venom MMP and the necessity of a nonphysiological (high-salt) environment] give an unprec-

¶[4-(*N*-Hydroxyamino)-2*R*-isobutyl-3*S*-(thiophen-2-ylthiomethyl)succinyl]-L-phenylalanine-*N*-methylamide.
‖[4-(*N*-Hydroxyamino)-2*S*-isobutyl-3*R*-(thiophen-2-ylthiomethyl)succinyl]-D-phenylalanine-*N*-methylamide.

**Because of sequence numbering differences, His-146 of Ht-d corresponds to His-118 (or 218) of MMP-1, His-202 (201) of MMP-3, or His-197 (117) of MMP-8, N-terminal enumeration being dependent upon individual expression systems.

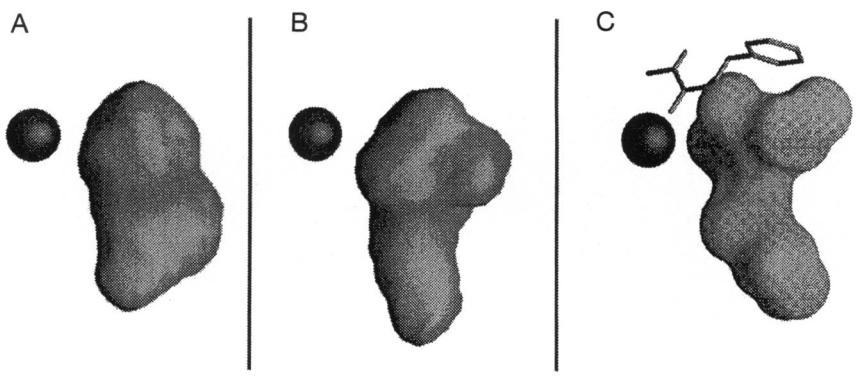

FIG. 4. Cartoon drawing of S1′ pocket shape for MMP-8 (*A*) and Ht-d (*B*) with the same orientation (Zn atom as a dark sphere). Molecular surface of the segment of BB-94 (*C*) inserted into the S1′ pocket. Measurement of the S1′ pocket volume and of the protein molecular surface reveals a significant difference between Ht-d (279.2 Å^3) and MMP-8 (226.5 Å^3). The volume occupied by the inserted BB-94 part is 253 Å^3, which suggests a possible 100% fit in Ht-d and an impossible fit in MMP-8 for the analyzed orientation of the inhibitor. Shapes and volumes have been calculated by using GRASP (27).

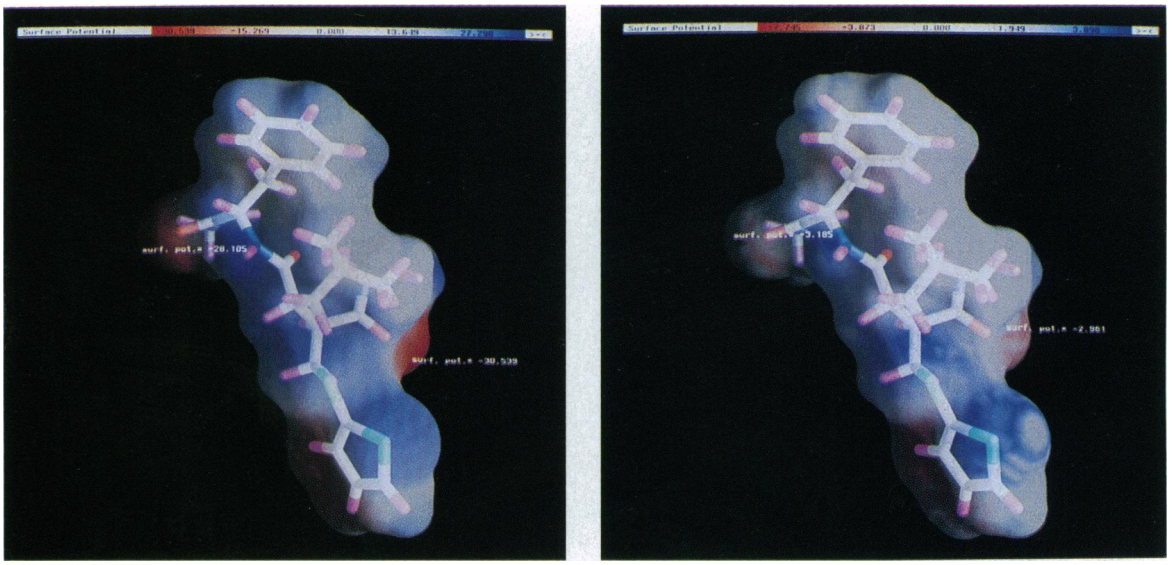

FIG. 5. Surface potential of BB-94 calculated with DELPHI (24). BB-94 is visible through the transparent molecular surface with the positive charges in blue and negative charges in red. (*Left*) In water at 0 M ionic strength. The maximum negative potential is localized on the oxygen atom of the hydroxamate ($-30.539\ kT/e$), while the carboxyl oxygen of Phe is less negative ($-28.105\ kT/e$). (*Right*) In a solution of 0.5 M ionic strength. The overall potential is reduced by an order of magnitude due to the screening effect of the ions, the hydroxamate oxygen becoming less negatively charged ($-2.961\ kT/e$) than the Phe carboxyl oxygen ($-3.185\ kT/e$).

edented result, the full occupancy of the S1′ primary specificity site. The crystallographic elucidation of BB-94 binding and subsequent molecular modeling show that the shared physiological activity of venom and mammalian proteinases as collagenases (10) has a strict structural basis (9, 14), confirming the relevance of this study. MMP inhibitors have potential therapeutic value in a number of pathologic conditions ranging from corneal ulceration to arthritis to cancer. Many of the metalloproteinase inhibitors thus far under investigation are based on substrate analogs, generally derivatized peptides. Common binding features include (*i*) Zn ligation, (with displacement of a catalytically essential water molecule at the apical locus), (*ii*) occupancy of subsites along the extended binding site (S, S′), and (*iii*) optimal occupancy of the primary specificity (S1′) site. Because the hydroxamate group precludes creation of inhibitors capable of binding to both S and S′ loci in the extended binding site, a comparable transition state analog complex (9) is noteworthy because it defines occupancy in both the S and S′ regions. From earlier studies of thermolysin inhibitors, the hydroxamate moiety was identified as a preferred Zn ligand (32), presenting a concept that continues to dominate the design of Zn proteinase inhibitors (7, 30), e.g., BB-94. While attention was directed to the large size of the S1′ primary specificity site, shown to contain a Leu side chain (7), this subsite has been more fully occupied (30%) by methyl-Tyr, Trp side chains (14), or homo-Phe (30). In the later case, the apical Zn ligand is the carboxylate group of Trp.

These crystallographic results reveal an unexpected inhibitor binding geometry, suggesting that although the hydroxamate moiety may be a better Zn ligand than the methylamide group under physiological conditions, in high (2.4 M) salt buffer, van der Waals interactions derived especially from the full insertion of the thiophene side chain into the cavernous S1′ pocket (Fig. 3) help shift the balance in favor of the reported complex. There is evidence suggesting that a fluorogenic substrate has reduced binding affinity to Ht-d in a high salt buffer environment, the electrostatic screening effect weakening the specific substrate–enzyme interactions. Work is in progress to fully explore the nature of ligand–enzyme interactions in such a nonphysiological environment, commonly employed in crystallization experiments.

Alternative binding modes are the exception in the structural literature (33). Conservative experimental methods were, therefore, employed in the soaking, active site modeling, and refinement of the title structure. While several MMP inhibitors, such as BB-94, have been designed intuitively, their specific mode of binding was an hypothesis subject to structural elucidation. At 2.0-Å resolution, this crystallographic analysis of a potent antitumor compound illustrates the utility of structural studies for illuminating the nature of alternative lock and key (34, 35) interactions and unambiguously depicts an unexpected binding geometry for BB-94, upon interaction with the active site of Ht-d. Because nature created and conserved an enormous S1′ pocket, could endogenous compounds be serving a physiological function, yet to be observed? These results point to possible pitfalls of molecular modeling prejudices (36) for the design of inhibitors and potential drugs. Structural optimization of ligand–receptor interactions simultaneously can provide increased specificity by using steric discrimination to differentiate among the several classes of matrix metalloproteinases.

We thank Dr. W. Stetler-Stevenson for useful discussions and Drs. K. Appelt and W. Bode for providing valuable coordinates. Dr. C. Blood helped with the affinity analysis. Prof. G. N. Phillips assisted with data collection. Partial funding was provided by the Robert A. Welch Foundation (E.F.M.) and the National Cancer Institute (L.A.L.).

1. Woessner, J. F., Jr. (1991) *FASEB J.* **5,** 2145–2154.
2. Stetler-Stevenson, W. G., Aznavoorian, S. & Liotta, L. A. (1993) *Annu. Rev. Cell Biol.* **9,** 541–573.
3. Brown, P. D., Bloxidge, R. E., Stuart, N. S. A., Gatter, K. C. & Carmichael, J. J. (1993) *J. Natl. Cancer Inst.* **85,** 574–587.
4. Brown, P. D., Bloxidge, R. E., Anderson, E. & Howell, A. (1993) *Clin. Exp. Metastasis* **11,** 183–189.
5. Albini, A., Melchiori, A., Santi, L., Liotta, L. A., Brown, P. D. & Stetler-Stevenson, W. G. (1991) *J. Natl. Cancer Inst.* **83,** 775–779.
6. Schnaper, H. W., Grant, D. S., Stetler-Stevenson, W. G., Fridman, R., D'Orazi, G., Murphy, A. N., Bird, R. E., Hoythya, M., Fuerst, T. R., French, D. L. & Liotta, L. A. (1993) *J. Cell. Physiol.* **156,** 235–246.
7. Borkakoti, N., Winkler, F. K., Williams, D. H., D'Arcy, A., Broadhurst, M. J., Brown, P. A., Johnson, W. H. & Murray, E. J. (1994) *Nat. Struct. Biol.* **1,** 106–110.

8. Becker, J. W., Marcy, A. I., Rokosz, L. L., Axel, M. G., Burbaum, J. J., Fitzgerald, P. M. D., Cameron, P. M., Esser, C. K., Hagmann, W. K., Hermes, J. D. & Springer, J. P. (1995) *Protein Sci.* **4,** 1966–1976.
9. Bode, W., Reinemer, P., Huber, R., Kleine, T., Schnierer, S. & Tschesche, H. (1994) *EMBO J.* **13,** 1263–1269.
10. Fox, J. W., Campbell, R., Beggerly, L. & Bjarnason, J. B. (1986) *Eur. J. Biochem.* **156,** 65–72.
11. Bode, W., Gomis-Rüth, R.-X. & Stöckler, W. (1993) *FEBS Lett.* **331,** 134–140.
12. Schechter, I. & Berger, A. (1967) *Biochem. Biophys. Res. Commun.* **27,** 157–162.
13. Gomis-Rüth, R.-X., Kress, L. F., Kellermann, J., Mayr, I., Lee, X., Huber, R. & Bode, W. (1994) *J. Mol. Biol.* **239,** 513–544.
14. Zhang, D., Botos, I., Gomis-Rüth, F.-X., Doll, R., Blood, C., Njoroge, F. G., Fox, J. W., Bode, W. & Meyer, E. F. (1994) *Proc. Natl. Acad. Sci. USA* **91,** 8447–8451.
15. Davies, B., Brown, P. D., East, N., Crimmin, M. J. & Balksill, F. R. (1993) *Cancer Res.* **53,** 2087–2091.
16. Chirvi, R. G. S., Garofalo, A., Crimmin, M. J., Bawden, L. J., Stoppacciaro, A., Brown, P. D. & Giavazzi, R. (1994) *Int. J. Cancer* **58,** 460–464.
17. Sledge, G. W., Jr., Quali, M., Goulet, R., Bone, E. A. & Fife, R. (1995) *J. Natl. Cancer Inst.* **87,** 1546–1550.
18. Grams, F., Crimmin, M., Hinnes, L., Huxley, P., Pieper, M., Tschesche, H. & Bode, W. (1995) *Biochemistry* **34,** 14012–14020.
19. Gewirth, D., Otwinowski, Z. & Minor, W. (1994) *The HKL Manual* (Yale Univ., Press, New Haven, CT), 3rd Ed.
20. Brünger, A. T., Kuriyan, J. & Karplus, M. (1987) *Science* **235,** 458–460.
21. Biosym Inc. (1993) MOPAC 6.0 from Insight II (Biosym Inc., San Diego), Version 2.3.0.
22. Laskowski, R. A., MacArthur, M. W., Moss, D. S. & Thornton, J. M. (1993) *J. Appl. Crystallogr.* **26,** 283–291.
23. Nicholls, A., Sharp, K. A. & Honig, B. (1991) *Proteins Struct. Funct. Genet.* **11,** 281–296.
24. Gilson, M. K., Sharp, K. A. & Honig, B. (1987) *J. Comput. Chem.* **9,** 327–335.
25. Stewart, J. J. P. (1990) *J. Comput.-Aided Drug Des.* **4,** 1–105.
26. Dewar, M. J. S. & Thiel, W. (1977) *J. Am. Chem. Soc.* **99,** 4899–4907.
27. Goodford, P. J. (1985) *J. Med. Chem.* **28,** 849–857.
28. Kraulis, P. J. (1991) *J. Appl. Crystallogr.* **24,** 946–950.
29. Botos, I., Scapozza, L., Shannon, J. D., Fox, J. W. & Meyer, E. F. (1995) *Acta Crystallogr. Sect. D* **51,** 597–604.
30. Porter, J. R., Beeley, N. R. A., Boyce, B. A., Mason, B., Millican, A., Millar, K., Leonard, J., Morphy, J. R. & O'Connell, J. P. (1994) *Bioorg. Med. Chem. Lett.* **4,** 2741–2746.
31. Meyer, E. (1992) *Protein Sci.* **1,** 1543–1562.
32. Powers, J. C. & Harper, J. W. (1986) in *Proteinase Inhibitors*, eds. Barret, A. J. & Salvensen, G. (Elsevier, Amsterdam), pp. 55–152.
33. Meyer, E. F., Botos, I., Scapozza, L. & Zhang, D. (1995) *Perspect. Drug Discovery Des.* **3,** 168–195.
34. Fischer, E. (1894) *Ber. Dtsch. Chem. Ges.* **27,** 2984–2993.
35. Meyer, E. F. (1995) *Pharm. Acta Helvet.* **69,** 177–183.
36. Bode, W., Meyer, E. F. & Powers, J. C. (1989) *Biochemistry* **28,** 1951–1963.